Detailed study of the Fermi surfaces of the type-II Dirac semimetallic candidates $X\mathrm{Te}_2$ (X=Pd, Pt)

W. Zheng,[1,2] R. Schönemann,[1,*] N. Aryal,[1,2] Q. Zhou,[1,2] D. Rhodes,[1,2,†] Y.-C. Chiu,[1,2] K.-W. Chen,[1,2] E. Kampert,[3] T. Förster,[3] T. J. Martin,[4] G. T. McCandless,[4] J. Y. Chan,[4] E. Manousakis,[1,2] and L. Balicas[1,2,‡]

[1]*National High Magnetic Field Laboratory, Florida State University, Tallahassee, Florida 32310, USA*

[2]*Department of Physics, Florida State University, Tallahassee, Florida 32306, USA*

[3]*Dresden High Magnetic Field Laboratory (HLD-EMFL), Helmholtz-Zentrum Dresden-Rossendorf, 01328 Dresden, Germany*

[4]*Department of Chemistry and Biochemistry, The University of Texas at Dallas, Richardson, Texas 75080, USA*

(Received 30 April 2018; published 29 June 2018)

We present a detailed quantum oscillatory study on the Dirac type-II semimetallic candidates PdTe_2 and PtTe_2 via the temperature and the angular dependence of the de Haas–van Alphen and Shubnikov–de Haas effects. In high-quality single crystals of both compounds, i.e., displaying carrier mobilities between 10^3 and 10^4 $\mathrm{cm}^2/\mathrm{Vs}$, we observed a large nonsaturating magnetoresistivity which in PtTe_2 at a temperature $T = 1.3$ K leads to an increase in the resistivity up to $(5 \times 10^4)\%$ under a magnetic field $\mu_0 H = 62$ T. These high mobilities correlate with their light effective masses in the range of 0.04 to 1 bare electron mass according to our measurements. For PdTe_2 the experimentally determined Fermi surface cross-sectional areas show excellent agreement with those resulting from band structure calculations. Surprisingly, this is not the case for PtTe_2, whose agreement between calculations and experiments is relatively poor even when electronic correlations are included in the calculations. Therefore, our study provides strong support for the existence of a Dirac type-II node in PdTe_2 and probably also for PtTe_2. Band structure calculations indicate that the topologically nontrivial bands of PtTe_2 do not cross the Fermi level ε_F. In contrast, for PdTe_2 the Dirac type-II cone does intersect ε_F, although our calculations also indicate that the associated cyclotron orbit on the Fermi surface is located in a distinct k_z plane with respect to that of the Dirac type-II node. Therefore, it should yield a trivial Berry phase.

DOI: 10.1103/PhysRevB.97.235154

I. INTRODUCTION

In the last few years, solid-state systems have emerged as promising candidates for searching for quasiparticles with properties akin to particles originally predicted in high-energy physics such as the Dirac, Weyl, and Majorana fermions. Massless Dirac fermions were discovered in graphene [1] and in the various topological insulators [2–4]. In these and in the so-called type-I Dirac semimetals [5], cone-shaped electron and hole bands meet at a single point in momentum space, i.e., the Dirac node. Unlike Dirac fermions that have been observed in particle physics, Weyl fermions have been discovered only recently as quasiparticles within certain semimetals, whose associated Weyl nodes emerge in pairs of opposite chirality, or topological charges, at linear touching points between electron and hole bands. Similar to type-I Dirac points, type-I Weyl points emerge when either inversion or time-reversal symmetry is broken, as in the TaAs family of compounds [6–8]. Recently, the existence of the so-called type-II Weyl and Dirac fermions which break Lorentz invariance and occur at the touching points between electron and hole pockets within the energy momentum dispersion associated with tilted Weyl or Dirac cones in k space was predicted [9]. Candidates predicted to display Weyl or Dirac type-II electronic dispersions are the transition-metal dichalcogenides like $(\mathrm{W,Mo})\mathrm{Te}_2$ [10,11] and the diphosphides $(\mathrm{Mo, W})\mathrm{P}_2$ [12–14].

The transition-metal dichalcogenides PdTe_2 and PtTe_2 crystalize in a layered CdI_2-type structure of the trigonal space group $P\bar{3}m1$ [15–17], which is shown in Figs. 1(a) and 1(b). The crystal has inversion symmetry; hence, the bands are Kramers degenerate. PdTe_2 and PtTe_2 as well as PtSe_2 are predicted to be the first candidates for the realization of Dirac type-II fermions based on first-principles calculations [18]. Recent publications claim to find experimental evidence for the existence of Dirac type-II points after mapping their electronic band structure via angle-resolved photoemission spectroscopy measurements [19–23] and after extracting the Berry phase from magnetization measurements [24]. Interestingly, in PdTe_2 Dirac type-I points are predicted to emerge upon application of hydrostatic pressure and to coexist with the type-II points within a certain range of pressures [25].

PdTe_2 undergoes a superconducting transition below $T_c = 1.7$ K, which in combination with topologically nontrivial bulk bands as well as topological surface states [23], would make this compound a promising candidate for a topologically nontrivial superconducting state. Notice that its superconducting transition temperature T_c can be increased up to 4.65 K by replacing a fraction of Pd with Au [26]. However, magnetization and transport measurements indicate that PdTe_2 is a type-I superconductor [27] with recent reports [28], including low-temperature scanning tunneling

*schoenemann@magnet.fsu.edu

†Present address: Department of Mechanical Engineering, Columbia University, New York, New York, USA.

‡balicas@magnet.fsu.edu

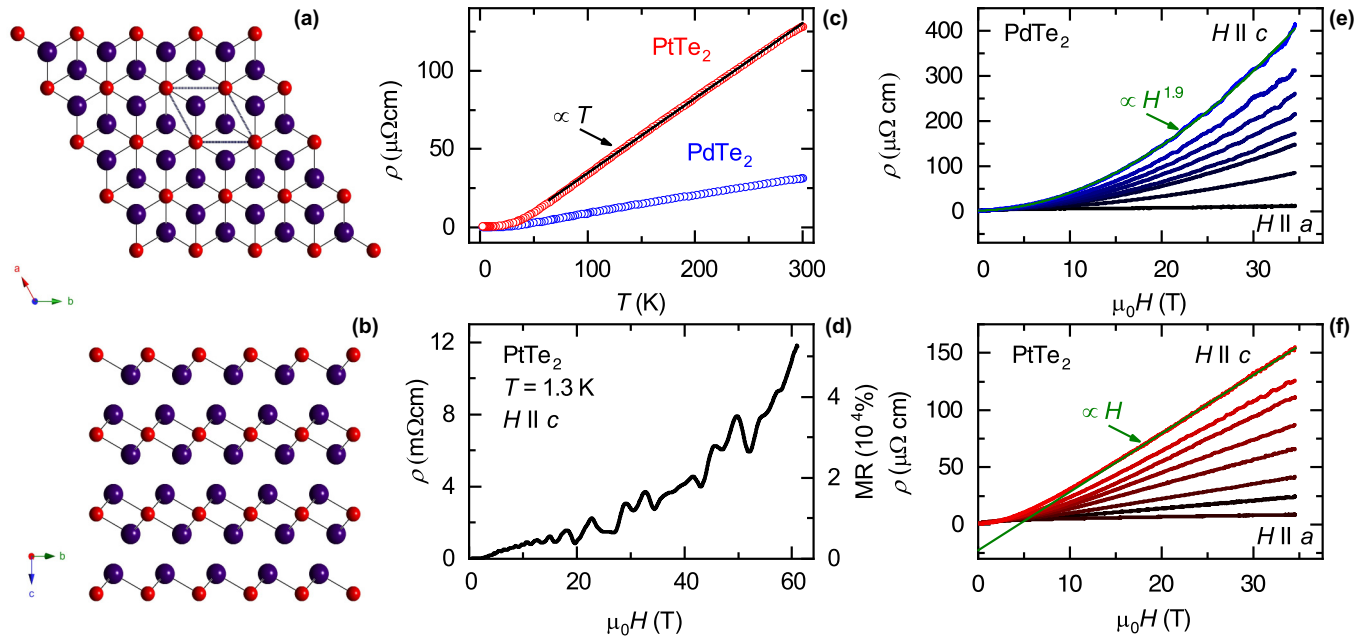

FIG. 1. (a) and (b) Crystallographic structure of $PdTe_2$ (and $PtTe_2$) via the atomic arrangements observed within the *ab* and *bc* planes, respectively. Here, the Pt/Pd and Te atoms are symbolized by red and blue spheres, respectively. The unit cell is indicated by the dashed line in (a). (c) Resistivity ρ as a function of the temperature for $PtTe_2$ and $PdTe_2$ (red and blue makers, respectively). The solid black line is a linear fit, indicating $\rho \propto T$ for $T \gtrsim 30$ K. (d) ρ as a function of the magnetic field $\mu_0 H$ for fields up to 62 T for a $PtTe_2$ single crystal at $T = 1.3$ K and for $\mu_0 H \parallel c$ axis, as measured under pulsed magnetic fields. Oscillations in $\rho(\mu_0 H)$ become markedly visible beyond $\simeq$10 T due to the SdH effect. (e) and (f) Magnetoresistivity curves for $PdTe_2$ (blue) and $PtTe_2$ (red) at $T = 0.35$ K and for various angles between $H \parallel c$ and $H \parallel a$. Green lines represent fits of the high-field data to a single power law $\rho(H) \propto H^{\alpha}$, yielding $\alpha = 1.9$ for $PdTe_2$ and $\alpha = 1$ for $PtTe_2$.

microscopy [29], claiming conventional superconductivity for this compound. Conventional *s*-wave superconductivity is also favored by recent heat-capacity measurements in $PdTe_2$ [30], suggesting that its bulk electronic structure might, in fact, not display topological character.

Although the magnetoresistance and magnetization measurements of both $PtTe_2$ and $PdTe_2$ have been reported in the last year [24,31], detailed information about the Fermi surface topography extracted from the angular dependence of bulk measurements like the de Haas–van Alphen (dHvA) and Shubnikov–de Haas (SdH) effects along with a comparison with density functional theory (DFT) calculations is still missing. Notice, for instance, that the initial report on the dHvA effect in $PdTe_2$ revealed just a few Fermi surface cross-sectional areas, e.g., only two small dHvA frequencies for fields along the *c* axis, which were claimed to be in broad disagreement with band structure calculations [32]. Here, we present a detailed Fermi surface (FS) study of both compounds through low-field magnetization and high-field electrical transport measurements in order to compare our experimental findings with first-principles band structure calculations. We find that DFT calculations describe the overall Fermi surface of $PdTe_2$ quite well, with some minor differences, but DFT provides a poor description of the FS of $PtTe_2$. Our measurements confirm the existence of tilted Dirac type-II cones in $PdTe_2$, which possibly also occur in $PtTe_2$. DFT also indicates for both compounds that the extremal cross-sectional areas of the Fermi surface detected by quantum oscillations ought to display a zero Berry phase despite previous claims in favor of a topologically nontrivial cyclotron orbit.

II. EXPERIMENT

High-quality single crystals of $PdTe_2$ were synthesized through a Te flux method: Pd (99.999%) and Te (99.999%) with an atomic ratio of 1:10 were sealed in an evacuated quartz ampule and subsequently heated to 800 °C and held at that temperature for 4 h. Then the ampule was slowly cooled to 525 °C at a rate of 1 °C/h. The excess Te was removed by centrifuging. The as-harvested single crystals were annealed for a few days at 520 °C to improve the sample quality and remove residual excess Te. The synthesis of $PtTe_2$ followed qualitatively the same heating and annealing procedure. Pt (99.999%) and Te (99.999%) in a ratio of 1:25 were heated up to 925 °C, slowly cooled down to 600 °C, and subsequently centrifuged. The synthesis yielded platelet-like, easily cleavable single crystals with the crystallographic *c* axis oriented perpendicularly to the largest surface of the platelet. The phase purity of these crystals was confirmed by single-crystal x-ray diffraction (see the Supplemental Material, Fig. S1 [33]) and energy-dispersive x-ray spectroscopy measurements.

Conventional magnetotransport experiments on $PdTe_2$ and $PtTe_2$ single crystals were performed in a physical property measurement system using a standard four-terminal method under magnetic fields up to $\mu_0 H = 9$ T and to temperatures down to $T = 1.8$ K. High-field magnetotransport experiments were performed in both a resistive Bitter magnet at the National High Magnetic Field Laboratory in Tallahassee, under continuous fields up to $\mu_0 H = 34.5$ T and temperatures down to $T \simeq 0.3$ K, and a pulsed magnet providing fields up to $\mu_0 H = 62$ T with a pulse duration of 150 ms at the

Dresden High Magnetic Field Laboratory. Magnetization measurements under fields up to $\mu_0 H = 7\,\mathrm{T}$ were performed in a commercial superconducting quantum interference device magnetometer. Additional transport measurements were conducted in a $\mu_0 H = 18\,\mathrm{T}$ superconducting magnet coupled to a dilution refrigerator. Magnetic torque measurements under pulsed magnetic fields were conducted with a piezoresistive microcantilever technique.

Electronic structure calculations were performed using the QUANTUM ESPRESSO package [34] within the generalized gradient approximation (GGA) with the inclusion of spin-orbit coupling (SOC). The structural parameters were taken from Ref. [35]. For the GGA+SOC calculations, fully relativistic norm-conserving pseudopotentials are generated using the optimized norm-conserving Vanderbilt pseudopotentials as described in Ref. [36]. The $5s$, $5p$, $5d$, and $6s$ electrons for Pt, the $4s$, $4p$, and $4d$ electrons of Pd, and the $4d$, $5s$, and $5p$ electrons for Te were treated as valence electrons. After rigorous convergence testing, the plane-wave energy cutoff was taken to be 60 Ry, and a k-point mesh of $11 \times 11 \times 8$ was used to sample the Brillouin zone. The Fermi surfaces were generated using a k-point mesh of $51 \times 51 \times 40$ and were visualized using the XCRYSDEN software [37]. The angular dependence was calculated using the SKEAF code [38]. In order to compare our band structure calculations with those in Refs. [23,29] we recalculated the band structure of $PdTe_2$ using the WIEN2K [39] implementation of DFT as used for both reports. We find that QUANTUM ESPRESSO and WIEN2K yield nearly identical band structures (see the Supplemental Material, Fig. S2 [33]). These differ considerably, e.g., in the number of band crossings and in the position of the Dirac type-II point, with respect to the calculations in Ref. [40].

III. RESULTS

Resistivity ρ measurements as a function of the temperature on annealed $PdTe_2$ and $PtTe_2$ single crystals are shown in Fig. 1(c). All samples show metallic behavior over the entire temperature range, albeit with an anomalous linear dependence on T above $T \simeq 30\,\mathrm{K}$. The large residual resistivity ratio $\rho(300\,\mathrm{K})/\rho(T \to 0\,\mathrm{K}) = 290$ for $PdTe_2$ and 220 for $PtTe_2$ and the corresponding low residual resistivities ρ_0 are strong evidence for the high quality of these crystals. Here, $\rho(300\,\mathrm{K})$ is the resistivity at 300 K, and $\rho(T \to 0\,\mathrm{K})$ is the residual resistivity in the limit of zero temperature as extracted from the resistivity data; $\rho(T)$ quickly saturates at the value of ρ_0 below $T = 30\,\mathrm{K}$. Notice that the best $PdTe_2$ crystals display $\rho_0 \simeq 0.1\ \mu\Omega\,\mathrm{cm}$, while one obtains $\simeq 0.5\ \mu\Omega\,\mathrm{cm}$ for $PtTe_2$. Notice also that neither compound displays Fermi liquid behavior or $\rho(T) \propto T^2$ since the low-temperature behavior corresponds to just a simple crossover from a linear temperature dependence to saturation of the resistivity upon cooling, yielding $\rho(T) \propto T^{\sim 3}$. Both compounds exhibit a large, nonsaturating, and anisotropic magnetoresistance (MR), as shown in Figs. 1(d) to 1(f). At $T = 2\,\mathrm{K}$ and under $\mu_0 H = 9\,\mathrm{T}$, the MR reaches a few thousand percent for fields applied along the crystallographic c axis. Its behavior can be described as a combination of a linear and quadratic in field terms: $\rho(H) = \rho(\mu_0 H = 0\,\mathrm{T}) + A\mu_0 H + B(\mu_0 H)^2$, with positive A and B coefficients. Unlike compensated semimetals [41], $PdTe_2$ and $PtTe_2$ do not show the conventional quadratic in field dependence, nor can their $\rho(\mu_0 H)$ be described by a single power law. Instead, one must include a linear-in-field component, as previously observed in Dirac systems upon approaching the quantum limit [42], to describe the magnetoresistive behavior observed under fields up to $\mu_0 H = 9\,\mathrm{T}$.

To gain further insight into the magnetoresistive behavior of $PtTe_2$, we conducted Hall-effect measurements under fields up to $\mu_0 H = 9\,\mathrm{T}$ and temperatures between 2 and 300 K. The results are displayed in Fig. S3 [33]. We extracted the electron and hole carrier densities n_e and n_h and their respective mobilities μ_e and μ_h from fittings of ρ_{xx} and ρ_{xy} to the two-band model [43–45]. At $T = 2\,\mathrm{K}$ the fits yield $n_\mathrm{e} = 8.8 \times 10^{20}\,\mathrm{cm}^{-3}$, $n_\mathrm{h} = 10.2 \times 10^{20}\,\mathrm{cm}^{-3}$, $\mu_\mathrm{e} = 0.55 \times 10^4\,\mathrm{cm}^2/\mathrm{V\,s}$, and $\mu_\mathrm{h} = 0.36 \times 10^4\,\mathrm{cm}^2/\mathrm{V\,s}$. These carrier mobilities are just a factor of $\sim$2 smaller than those of WTe_2 [44] but one order of magnitude smaller when compared to those of γ-$MoTe_2$ [11,45], which we tentatively attribute to a more effective carrier backscattering by impurities, although all of these systems display comparable residual resistivities. Interestingly, for $PtTe_2$ we found the difference between the densities of holes and electrons to be larger than 10%, particularly at low temperatures where the fits to the two-band model yield more accurate results. This indicates that charge-carrier compensation is not the leading mechanism producing the large magnetoresistivity observed in this compound, as claimed to be the case for other semimetals like WTe_2 and $MoTe_2$ [10,11], $PtBi_2$ [46], and W/MoP_2 [13,14]. Remarkably, transport measurements in $PtTe_2$ provide no evidence for saturation either, even under pulsed fields as high as $\mu_0 H = 62\,\mathrm{T}$ applied along its c axis [Fig. 1(d)]. For $PdTe_2$ we observe no saturation in the magnetoresistivity under fields as high as 35 T [see Fig. 1(e)]. Reliable Hall-effect data for this compound will be presented elsewhere.

Given the presence of Dirac type-II points within the electronic structure of both compounds, one might expect to detect charge carriers characterized by topologically nontrivial Berry phases [19–22,24]. In fact, $PdTe_2$ was already claimed to be topologically nontrivial [24] despite the DFT calculations (see Supplemental Material [33]) placing the Dirac type-II nodes deep below the Fermi level at -0.51 eV (-0.65 eV for $PtTe_2$). This is surprising since one might expect that the associated orbit might be located within a quadratically dispersing portion of the electronic band. But the authors of Ref. [24] extract a Berry phase $\phi_B \simeq \pi$ from the dHvA oscillations superimposed on the magnetization through the phase factor embedded within the Lifshitz-Kosevich (LK) formalism (see Ref. [47] and also [4]). The LK formula describes the quantum oscillatory phenomena observed in density-of-states-dependent physical variables such as the magnetization M through

$$\Delta M \propto -B^{1/2} R_T R_\mathrm{D} R_S \sin\left\{2\pi\left[\frac{F}{B} - \left(\frac{1}{2} - \phi\right)\right]\right\}, \quad (1)$$

where $R_T = \lambda T/\sinh(\lambda T)$ is the temperature damping factor, $R_D = \exp(-\lambda T_\mathrm{D})$, with $\lambda = 2\pi^2 k_\mathrm{B}\mu/\hbar e B$, is the Dingle damping factor, and R_S is the spin-damping factor [47]. The phase factor $\phi = \phi_\mathrm{B}/2\pi - \delta$ contains the Berry phase ϕ_B and a second phase shift δ which takes values of 0 or $\pm 1/8$ (the sign depends upon the cross-sectional area, i.e., maxima or minima) for Fermi surfaces with two- and three-dimensional

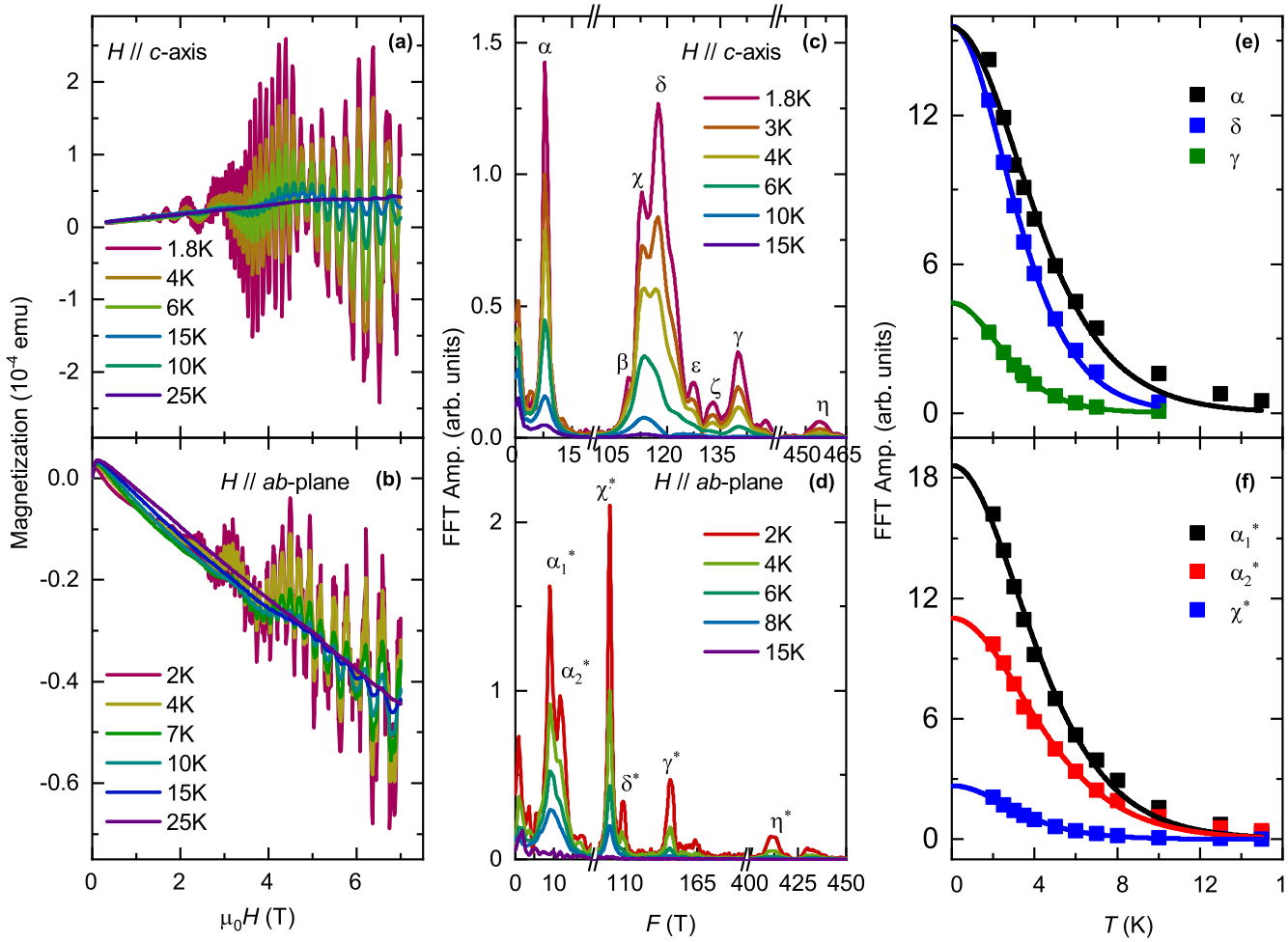

FIG. 2. (a) and (b) Magnetization of $PdTe_2$ as a function of the magnetic field for two different field orientations and for several temperatures between $T = 1.8$ and 25 K. (c) and (d) The corresponding fast Fourier transforms (FFTs). Peaks corresponding to extremal cross sectional areas of the Fermi surface are labeled with Greek letters. (e) and (f) Amplitude of the main peaks observed in the FFT spectra as a function of T, where solid lines represent fittings of the experimental data by the temperature damping factor within the Lifshitz-Kosevich formalism.

character, respectively. T_D is the sample-dependent Dingle temperature, and μ is the effective cyclotron mass. To probe the topological character of these compounds and check the claims of Ref. [24], we measured the magnetization M of $PdTe_2$ as a function of field $\mu_0 H$ for two field orientations, i.e., $H \parallel c$ and $H \parallel a$, as shown in Figs. 2(a) and 2(b), respectively. Similar measurements for $PtTe_2$ can be found in Fig. S4 [33]. The fast Fourier transforms (FFT) associated with the dHvA oscillations superimposed on $M[(\mu_0 H)^{-1}]$ are shown in Figs. 2(c) and 2(d) for both orientations. Several peaks are observable at frequencies F between 8 and 500 T for either field orientation. In general, to extract the Berry phase associated with each individual orbit one would have to fit $\Delta M(\mu_0 H)$ to a superposition of LK oscillatory terms, i.e., one for each cyclotron frequency. However, the large number of frequencies observed here (seven to eight) makes it nearly impossible to reliably extract the Berry phase for individual orbits given that each LK component requires several input parameters (i.e., amplitude, frequency, phase, effective mass, quantum lifetime, etc.). Instead, we chose to apply a low-pass filter around $F = 50$ T to extract only the oscillations associated with the α orbit ($F_\alpha = 8$ T). The results are shown in the top panel of Fig. 3. As discussed in Ref. [48], the minima in the oscillatory dHvA signal can be assigned to Landau indices $n - 1/4$, which produces the Landau fan diagram shown in the bottom panel of Fig. 3. An extrapolation of the fan diagram to $1/(\mu_0 H) \to 0$ leads to an intercept of 0.445, which is very close to the value of 0.46 reported by Ref. [24]. From $(\phi_B/2\pi \pm \delta) = 0.445$ one obtains ϕ_B values of $(2\pi \times 0.57)$ and $(2\pi \times 0.32)$, respectively, both not equal to the value of $(2\pi \times 0.46 \sim \pi)$ reported by Ref. [24].

We cross-checked our Berry phase extraction procedure by analyzing the oscillatory data collected from $PtTe_2$, obtaining the respective ϕ_B values for the α orbit which band structure calculations associate with topologically trivial electron pockets. This frequency is easy to separate from the other frequencies present in the FFT spectra, particularly for fields along a planar direction, and does yield a topologically trivial Berry phase (see Fig. S5 [33]). Nevertheless, it is important to emphasize that one should be particularly careful when extracting ϕ_B for both compounds given their large spin-orbit coupling and concomitant Landé g factors, which leads to a pronounced spin-dephasing term R_S. This is illustrated by Fig. S6 in the Supplemental Material [33], which reveals the

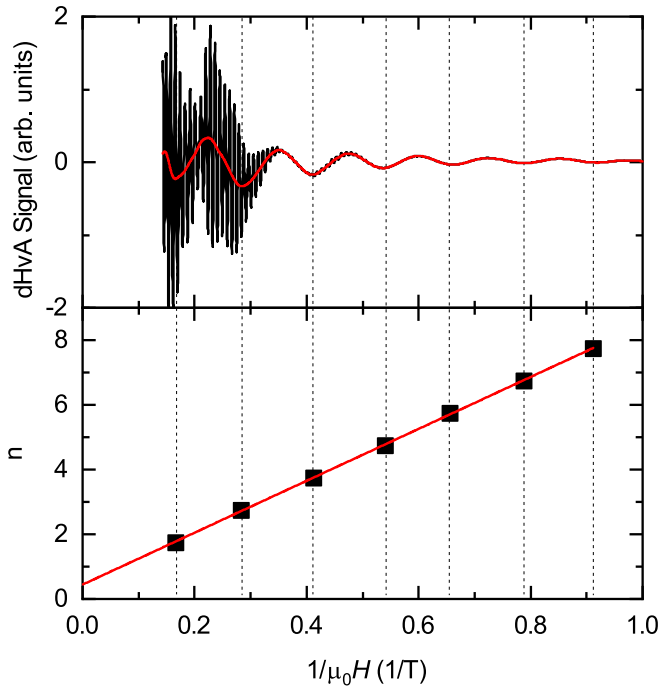

FIG. 3. Top: The black line represents the raw oscillatory dHvA signal of $PdTe_2$ for $H \parallel c$. The oscillations at the lowest α frequency with $F_\alpha = 8$ T can be separated by applying a low-pass filter at $F = 50$ T. The resulting oscillatory signal is shown as a solid red line. Bottom: Landau fan diagram of the α orbit.

TABLE I. Effective masses of $PdTe_2$ and $PtTe_2$ from magnetization and transport measurements.

$PdTe_2$, $H \parallel c$			$PdTe_2$, $H \parallel a$			
Orbit	$F(T)$	μ/m_0	Orbit	$F(T)$	μ/m_0	Band
α	8	0.045	α_1^*	9	0.051	3
β	109	0.039	α_2^*	12	0.048	2/4
χ	113	0.045	χ^*	99	0.065	2/4
δ	117	0.058	δ^*	106	0.041	2/4
ϵ	127	0.056				2/4
ζ	133	0.060				2/4
γ	140	0.069	γ^*	145	0.077	2/4
η	455	0.075	η^*	412	0.079	1
τ	920	1.49				3
ϕ	2350	0.56				3
κ	2675	0.69				3
λ	3534	0.74				2
ν	5324	1.16				3
$PtTe_2$, $H \parallel c$			$PtTe_2$, $H \parallel a$			
Orbit	$F(T)$	μ/m_0	Orbit	$F(T)$	μ/m_0	Band
α	100	0.11	α^*	123	0.15	2
β	107	0.11				2
γ	243	0.27	γ^*	209	0.25	2
δ	1703	1.6(2)				2
χ	1971	1.6(2)				2
ϕ	6068	3.6(8)				3

existence of the so-called spin zeros, or zero-amplitude oscillatory signals at specific angular values where $\cos(\pi g\mu/2m_0) = 0$, which occur whenever $(\pi g\mu/2m_0) = (n + 1/2)\pi$. It turns out that one observes two spin zeros for the β orbit of $PdTe_2$ which one should assign to $n = 0$ and $n = 1$, yielding $g_\beta^{n=0} \simeq 25.6$ and $g_\beta^{n=1} \simeq 77$, respectively, for $\mu/m_0 = 0.039$ (see Table I). These values point towards very large and anisotropic g factors for the smaller cyclotron orbits of $PdTe_2$ and hence to a pronounced modulation in the sign of R_S upon rotation, as previously observed by us in the MAl_3 compounds [49]. Given that Pt is a $5d$ element, one would expect an even larger spin-orbit coupling in $PtTe_2$, although the quality of our data does not clearly expose its spin zeros. Therefore, it is likely that the values of $\phi_B = (2\pi \times 0.57)$ and $\phi_B = (2\pi \times 0.46)$ obtained by us and reported by Ref. [24], respectively, both close to π, result from the modulation of the spin-dephasing factor.

The effective cyclotron masses for both $PdTe_2$ and $PtTe_2$ were determined from the amplitude of the dHvA and/or the SdH oscillations as a function of the temperature. Lower dHvA frequencies become clearer in the magnetization measurements when $\mu_0 H \lesssim 7$ T (see Figs. 2 and S4). Depending on the orientation of the field, $PdTe_2$ and $PtTe_2$ show either a paramagnetic or a diamagnetic background signal with superimposed quantum oscillations, indicating a rather anisotropic spin susceptibility. The effective masses μ_i can be extracted from the temperature dependence of the FFT amplitude of each individual peak by fitting the experimental data to the R_T term in the LK formalism, as shown in Figs. 2(e) and 2(f). The effective masses associated with higher frequencies were obtained by analyzing the amplitude of the oscillations observed in transport experiments performed under high magnetic fields (see Figs. 4 and 5). The extracted effective masses are summarized in Table I.

From the magnetization of $PdTe_2$ and for both field orientations, we extract very light effective masses, i.e., between $0.039m_0$ and $0.075m_0$ for those orbits with frequencies below 500 T. Higher frequencies like $F_\tau = 920$ T and $F_\phi = 2350$ T yield effective masses of $\mu_\tau = 1.49m_0$ and $\mu_\phi = 0.56m_0$ and can be observed in the high-field resistivity data for $H \parallel c$. They can be assigned to the larger hole pocket at the center of the Brillouin zone (band 3). $PtTe_2$ exhibits effective masses of $0.11m_0$ and $0.27m_0$ for the low frequencies α, β, and γ, also with similar values for both field orientations. The δ, χ, and ϕ orbits, which can be assigned to the large electron and hole pockets (bands 2 and 3), lead to higher frequencies ranging between 1703 and 6068 T which display larger effective masses with values between $1.6m_0$ and $3.6m_0$.

The angular dependence of the frequencies extracted from the quantum oscillatory phenomena observed in $PdTe_2$ and $PtTe_2$, as well as the angular dependence of the FS cross-sectional areas according to the DFT calculations, are shown in Fig. 6 (see also Fig. S7 [33]). Most of the frequencies were extracted from the FFT of the oscillatory signal superimposed on the resistivity measured at $T \simeq 25$ mK and under fields up to 18 T. The agreement between the DFT calculations and the experimental data for $PdTe_2$ is remarkable, in particular for the η, χ, and δ orbits resulting from electron bands 1 and 2. The larger λ orbit can be observed only for magnetic fields aligned nearly along the c direction. This is also the case for the ϕ, κ, and ν orbits, which can be assigned to the large open hole pocket at the center of the Brillouin zone (band 3).

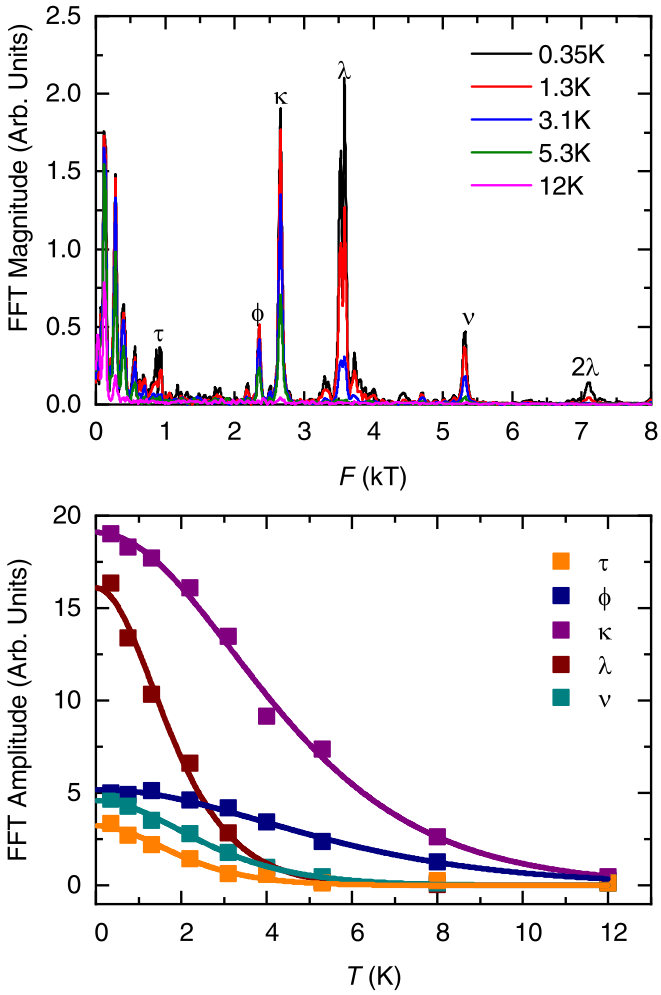

FIG. 4. Top: Fast Fourier transform (FFT) of the oscillatory component superimposed on $\rho(\mu_0 H)$ of $PdTe_2$ [see Fig. 1(e)] for $\mu_0 H \parallel c$ axis under temperatures T ranging between 0.35 and 12 K. Peaks correspond to the extremal cross-sectional areas of the Fermi surface, which are labeled with the Greek letters τ, ϕ, κ, λ, and ν. Bottom: amplitude of each peak/orbit observed in the FFT spectra as a function of T, where the solid lines are fits to the temperature damping factor R_T in the LK formalism.

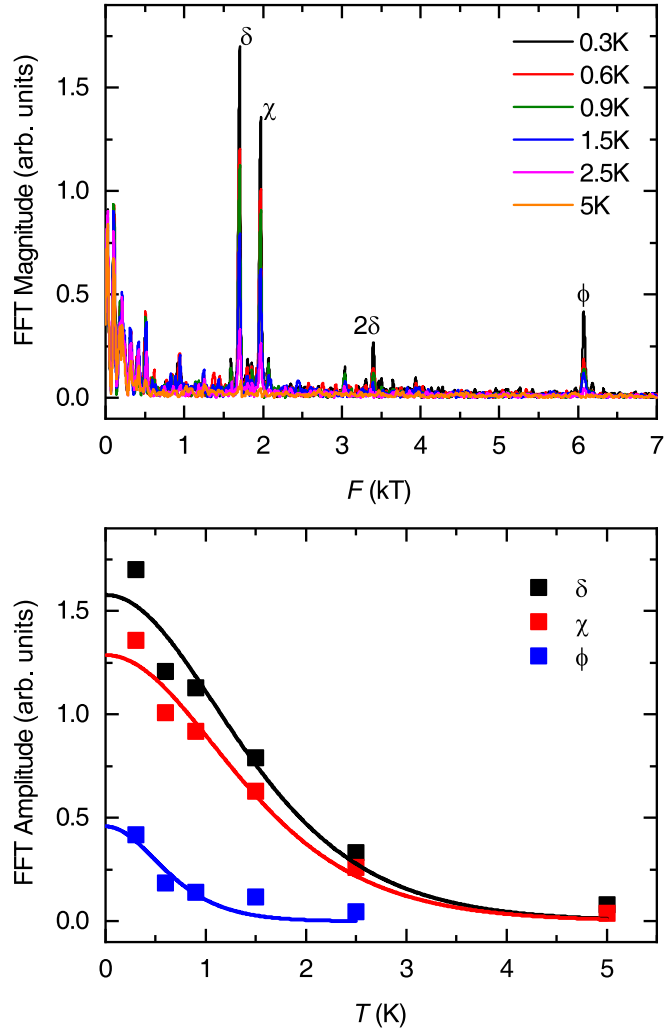

FIG. 5. Top: FFT of the oscillatory signal superimposed on $\rho(\mu_0 H)$ for $PtTe_2$ [see Fig. 1(f)] for $H \parallel c$ at temperatures between 0.35 and 5 K. Greek letters δ, χ, and ϕ label the individual peaks associated with the extremal cross-sectional areas of the Fermi surface. Bottom: Amplitude of each peak observed in the FFT spectra as a function of the temperature, where solid lines represent fits to the temperature damping factor R_T in the LK formalism.

For the lowest of the detected frequencies ($F \approx 8$ T) labeled as the α orbit, which can be assigned to the small satellite pockets resulting from band 3, there is a sizable mismatch between calculations and experiments. This disagreement is not surprising given that very small pocket areas like these tend to be very sensitive to small displacements in the Fermi level or in the precise position of the individual electronic bands which are within the energy resolution of the different DFT implementations.

In the case of $PtTe_2$, the experimental data cannot be as well described by the calculations following the QUANTUM ESPRESSO implementation of DFT. Band 1, which creates nearly spherical hole surfaces at the edges of the Brillouin zone like in $PdTe_2$, can be assigned to the γ frequency, which has a nearly flat angular dependence, but with a value of ~200 T, instead of 325 T as predicted by DFT. In the region near 100 T we observe two frequencies, α and β, which nearly match those of the smaller pockets in band 2. Some of the frequencies above 500 T associated with the more complexly shaped electron pockets of band 2 at the edge of the Brillouin zone can be matched with the δ and χ peaks observed when the field is nearly parallel to the c or a axis. Given that the γ and ϕ frequencies can be assigned to pockets in bands 1 and 3, one could increase the size of the hole sheets and decrease the size of the electron ones by lowering the Fermi energy, which should improve the match between experiments and the calculations. However, we are not able to observe via torque measurements a series of frequencies predicted within the range of 100 and 500 T under either static or higher pulsed fields. This might indicate that the shape of the Fermi surface is actually less complex than the predicted one. We confronted a similar situation when studying the Fermi surface of orthorhombic γ-$MoTe_2$ by observing a much simpler FS than the one extracted from angle-resolved photoemission

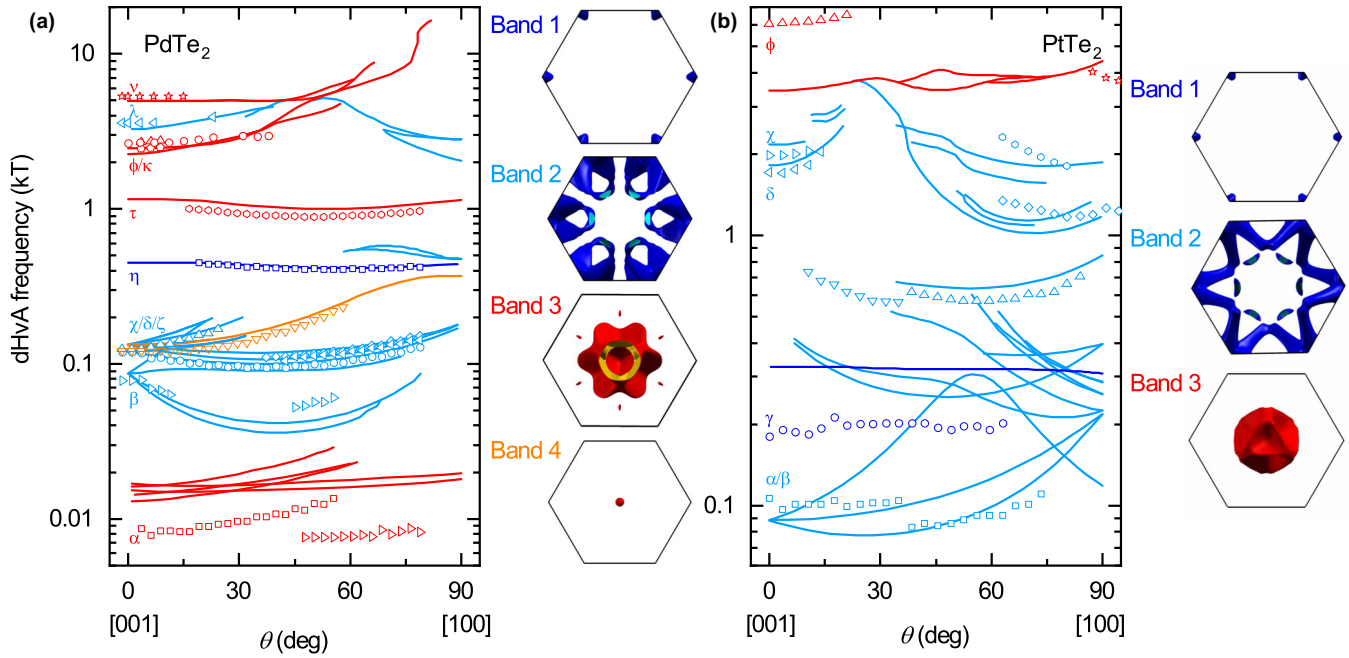

FIG. 6. Quantum oscillatory frequencies as a function of the angle θ between $\mu_0 H$ and the c axis as extracted from (a) $PdTe_2$ and (b) $PtTe_2$ single-crystals and for fields rotating between $\mu_0 H \parallel c$ axis and $\mu_0 H \parallel a$ axis. Symbols represent the experimental frequencies, while solid lines depict their angular dependence according to the DFT calculations. For $PdTe_2$ bands 1 (dark blue) and 2 (light blue) yield electronlike Fermi surface sheets, while bands 3 (red) and 4 (orange) lead to hole pockets. The same color scheme is used for the bands of $PtTe_2$. The corresponding Fermi surfaces within the hexagonal first Brillouin zone are displayed adjacent to each graph.

spectroscopy [11]. Our unpublished calculations indicate that this discrepancy results from electronic correlations, which motivated us to evaluate the role of correlations on the electronic structure and concomitant Fermi surface of $PtTe_2$.

IV. DISCUSSION

A. GGA+U calculations for $PtTe_2$

As previously discussed, Fig. 6 compares the angular dependence between the calculated and experimentally measured Fermi surface cross-sectional areas from quantum oscillation experiments. In contrast to $PdTe_2$, the agreement for $PtTe_2$ is far from excellent. Notice for example, that the orbit at around 6000 T is underestimated in the DFT calculations.

This orbit results from the large hole band centered around the Γ point. Within the GGA+SOC+U framework we have evaluated whether the reason for this discrepancy, in the case of the $PtTe_2$ compound, results from electronic correlations. Therefore, we used 2 and 4 eV for the value of an on-site Hubbard U on the Pt d orbital. But as seen in Figs. 7(a) and 7(b), respectively, for this range of U, we do not see any significant difference between band structures (with and

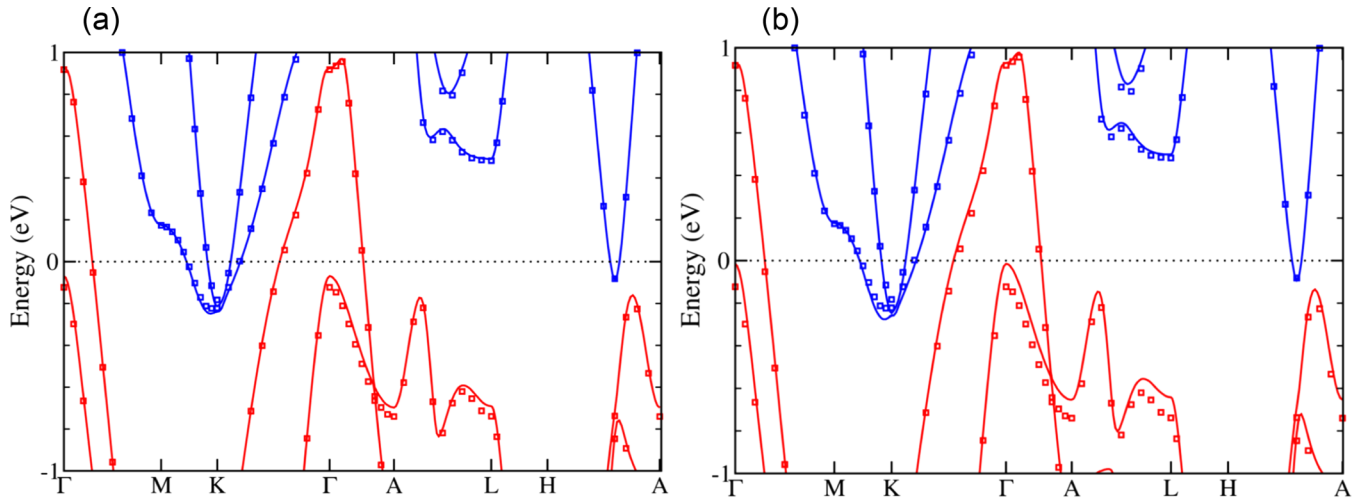

FIG. 7. (a) and (b) Band structure of $PtTe_2$ with spin-orbit coupling (SOC) when adding an on-site Hubbard U on the Pt d site for the cases $U = 2$ and 4 eV, respectively. The open circles show the bands without U.

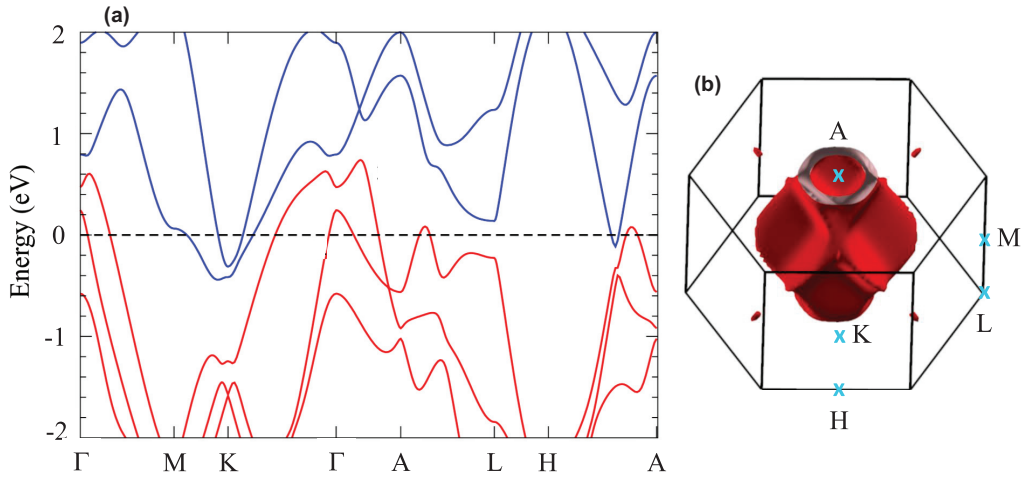

FIG. 8. (a) Band structure of $PdTe_2$. A transversal cut of the Dirac type-II cone is observed along the Γ-A direction with the node located at ~ -0.5 eV. Notice that it disperses all the way up to the Fermi level. (b) Holelike Fermi surfaces within the first Brillouin zone. A large hole sheet, responsible for the τ orbit, encloses the Γ-A direction along which the Dirac node is located. Light blue crosses indicate the high-symmetry points within the Brillouin zone.

without correlations) around the Fermi level. Therefore, the origin of this discrepancy between the calculated orbits and the experimentally measured ones remains to be resolved. Notice from Fig. 7 that the bands crossing at ~ -0.5 eV, thus forming the Dirac type-II cone (located along the line from Γ to A), do not disperse all the way up to ε_F. Therefore, the entirety of the Dirac cone does not intersect the Fermi level, implying that $PtTe_2$ should, according to DFT, *not* display topologically protected charge carriers. Subsequently, we discuss the case of $PdTe_2$, whose Dirac type-II cone does intersect ε_F (see Fig. 8).

B. Dirac point and Berry phase in $PdTe_2$

Our quantum oscillatory study does concede the possibility of a Berry phase being relatively close to π but only for the orbit of size ∼10 T and for magnetic fields parallel to the c axis. From its angular dependence we identified it with the small ellipsoidlike orbit of around 20 T, according to our DFT calculations [see Fig. 8(a)], which is seen in our Fermi surface calculations in Fig. 8(b) as the four small ellipsoidlike pockets. In addition, the two-dimensional band surfaces near this pocket are shown by the small "islands" in Fig. 9. However, as we

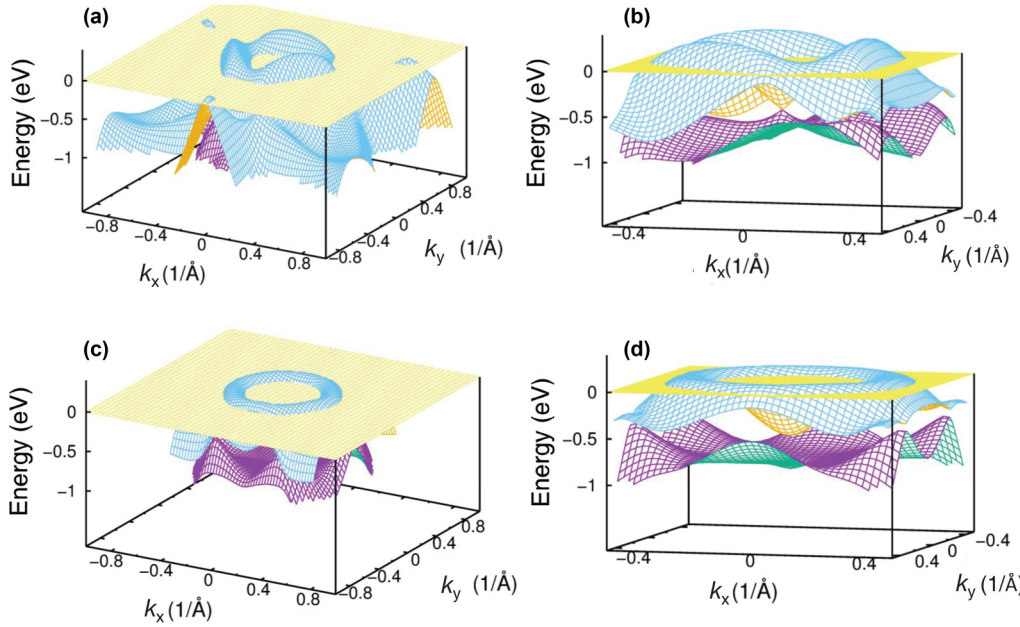

FIG. 9. Two-dimensional band structure of $PdTe_2$ within the k_x-k_y plane for different values of k_z. (a) and (b) The bands at a value of k_z where the Dirac point occurs (i.e., at $k_z = k_z^{\mathrm{DP}}$). (c) and (d) The bands for k_z corresponding to the extremum orbit, i.e., the τ orbit, close to the Dirac point ($k_z = 0.5 \times 2\pi/c$). Notice that the small islands in (a) have an area of ≈ 20 T. These islands appear only for k_z values in the close vicinity of the k_z^{DP}.

discuss below, there is no reason to expect a nontrivial topology in this case. Furthermore, the extraction of Berry phase by quantum oscillation experiments in the case of systems which possess both time-reversal symmetry and inversion symmetry is plagued by the issues discussed in Ref. [49]. As has been previously discussed, there is a type-II Dirac point (DP) which is shown in Fig. 8 along the Γ-A line at about 0.5 eV below the Fermi surface. The k_z value corresponding to the position of this DP is found to be $0.4 \times 2\pi/c$, which we will refer to as k_z^{DP}.

Since the position of the DP is about -0.5 eV from the Fermi level ε_F, the detection of a Berry phase of $\sim\pi$ in other reports [24] is surprising and hence deserves further investigation. In Fig. 9 we present the two-dimensional bands in the k_x-k_y plane for two values of k_z. First, in Fig. 9(a) [Fig. 9(b) is a zoomed-in version], the k_z value is fixed at k_z^{DP} and shows a type-I Dirac point at (0,0). Figure 9(c) [Fig. 9(d) is a zoomed-in version] presents the two-dimensional band structure for $k_z = 0.5 \times 2\pi/c$, a value of k_z where an extremal orbit exists and was observed by our quantum oscillatory experiments, i.e., the τ orbit in Fig. 6. Notice that a gap of approximately 0.4 eV appears for this value of k_z. As noted in the Supplemental Material of Ref. [49], an orbit situated slightly away from the DP can yield zero effective Berry phase in quantum oscillation experiments. Hence, this τ orbit is expected to yield a trivial Berry phase in such experiments, as the distance with respect to the DP is considerable and leads to a large energy gap. For reasons that remain unclear to us and as seen in Fig. 6, the τ orbit is not detectable for fields oriented nearly along the a or c crystallographic axis.

The small islands at ε_F in Fig. 9(a), which correspond to the previously discussed small ellipsoidlike Fermi surface pockets seen in Fig. 8(b), exist only for a k_z value in close proximity to k_z^{DP} and have a maximum size at k_z^{DP}. However, these islands emerge from a quadratic dispersion with a very distant connection to the Dirac type-II point. Therefore, this orbit must also be topologically trivial.

V. SUMMARY

To summarize, we performed a detailed study of the quantum oscillatory phenomena observed in the Dirac type-II semimetallic candidates $PdTe_2$ and $PtTe_2$. We obtained very light effective masses, in the range of 0.04 to 1.5 electron mass for $PdTe_2$ and from $0.11m_0$ to $3.6m_0$ for $PtTe_2$, concomitant high mobilities on the order of 5×10^3 cm^2/V s, and remarkably good agreement between density functional theory calculations and the topography of the Fermi surface of $PdTe_2$ as determined experimentally. Such agreement implies that this compound indeed displays a Dirac type-II node located at $\sim$0.5 eV below the Fermi level. The agreement between the DFT calculations and the Fermi surface cross-sectional areas of $PtTe_2$ is relatively poor, although it does *not* indicate a radical difference between the topographies of the calculated and of the experimentally determined Fermi surfaces. This suggests that this compound is also a good candidate for the existence of a Dirac type-II cone. However, in $PtTe_2$ electronic band calculations indicate that the Dirac type-II cone would not intersect its Fermi level or that this compound would be characterized by topologically trivial charge carriers. Although the calculations indicate that the Dirac cone does intersect ε_F in the case of $PdTe_2$, the associated orbit or Fermi surface cross-sectional area detected by quantum oscillations would be located on a different k_z plane with respect to the plane of the Dirac type-II node. This small displacement is enough to lead to a Berry phase $\phi_{\mathrm{B}} < \pi/2$ associated with topologically trivial [49] electronic orbits in $PdTe_2$. This is consistent with several recent reports claiming conventional superconductivity for $PdTe_2$. Nevertheless, it is still possible for $PdTe_2$ to display topologically nontrivial orbits at the Fermi level that would not coincide with the extremal cross-sectional areas detected by quantum oscillatory phenomena. Finally, we found that the small cyclotron orbits in $PdTe_2$ display large Landé g factors which lead to a pronounced angular dependence of the spin-dephasing factor in the Lifshitz-Kosevich formula. This could produce a spurious nontrivial Berry phase, as reported by other groups.

ACKNOWLEDGMENTS

This work was supported by DOE-BES through Award No. DE-SC0002613. J.Y.C. acknowledges support from NSF through Grant No. DMR-1700030. We acknowledge the support of the HLD-HZDR, a member of the European Magnetic Field Laboratory (EMFL). The National High Magnetic Field Laboratory is supported by the National Science Foundation through NSF/DMR-1644779 and the State of Florida.

[1] K. S. Novoselov, A. K. Geim, S. V. Morozov, D. Jiang, M. I. Katsnelson, I. V. Grigorieva, S. V. Dubonos, and A. A. Firsov, Nature (London) **438**, 197 (2005).

[2] H. Zhang, C.-X. Liu, X.-L. Qi, X. Dai, Z. Fang, and S.-C. Zhang, Nat. Phys. **5**, 438 (2009).

[3] S. M. Young, S. Zaheer, J. C. Y. Teo, C. L. Kane, E. J. Mele, and A. M. Rappe, Phys. Rev. Lett. **108**, 140405 (2012).

[4] Y. Ando, J. Phys. Soc. Jpn. **82**, 102001 (2013), and references therein.

[5] Z. J. Wang, H. M. Weng, Q. S. Wu, X. Dai, and Z. Fang, Phys. Rev. B **88**, 125427 (2013).

[6] S.-Y. Xu, I. Belopolski, N. Alidoust, M. Neupane, G. Bian, C. Zhang, R. Sankar, G. Chang, Z. Yuan, C.-C. Lee, S.-M. Huang, H. Zheng, J. Ma, D. S. Sanchez, B. Wang, A. Bansil, F. Chou, P. P. Shibayev, H. Lin, S. Jia, and M. Z. Hasan, Science **349**, 613 (2015).

[7] B. Q. Lv, H. M. Weng, B. B. Fu, X. P. Wang, H. Miao, J. Ma, P. Richard, X. C. Huang, L. X. Zhao, G. F. Chen, Z. Fang, X. Dai, T. Qian, and H. Ding, Phys. Rev. X **5**, 031013 (2015).

[8] H. Weng, C. Fang, Z. Fang, B. A. Bernevig, and X. Dai, Phys. Rev. X **5**, 011029 (2015).

[9] A. A. Soluyanov, D. Gresch, Z. Wang, Q. Wu, M. Troyer, X. Dai, and B. A. Bernevig, Nature (London) **527**, 495 (2015).

[10] M. N. Ali, J. Xiong, S. Flynn, J. Tao, Q. D. Gibson, L. M. Schoop, T. Liang, N. Haldolaarachchige, M. Hirschberger, N. P. Ong, and R. J. Cava, Nature (London) **514**, 205 (2014).

[11] D. Rhodes, R. Schönemann, N. Aryal, Q. Zhou, Q. R. Zhang, E. Kampert, Y.-C. Chiu, Y. Lai, Y. Shimura, G. T. McCandless, J. Y. Chan, D. W. Paley, J. Lee, A. D. Finke, J. P. C. Ruff, S. Das, E. Manousakis, and L. Balicas, Phys. Rev. B **96**, 165134 (2017).

[12] G. Autès, D. Gresch, M. Troyer, A. A. Soluyanov, and O. V. Yazyev, Phys. Rev. Lett. **117**, 066402 (2016).

[13] R. Schönemann, N. Aryal, Q. Zhou, Y.-C. Chiu, K.-W. Chen, T. J. Martin, G. T. McCandless, J. Y. Chan, E. Manousakis, and L. Balicas, Phys. Rev. B **96**, 121108(R) (2017).

[14] N. Kumar, Y. Sun, N. Xu, K. Manna, M. Yao, V. Süss, I. Leermakers, O. Young, T. Förster, M. Schmidt, H. Borrmann, B. Yan, U. Zeitler, M. Shi, C. Felser, and C. Shekhar, Nat. Commun. **8**, 1642 (2017).

[15] E. Revolinsky, E. Lautenschlager, and C. Armitage, Solid State Commun. **1**, 59 (1963).

[16] S. Furuseth, K. Selte, A. Kjekshus, S. Gronowitz, R. A. Hoffman, and A. Westerdahl, Acta Chem. Scand. **19**, 257 (1965).

[17] J. Mangin and P. Veber, J. Cryst. Growth **310**, 3077 (2008).

[18] H. Huang, S. Zhou, and W. Duan, Phys. Rev. B **94**, 121117(R) (2016).

[19] Y. Liu, J.-Z. Zhao, L. Yu, C.-T. Lin, A.-J. Liang, C. Hu, Y. Ding, Y. Xu, S.-L. He, L. Zhao, G.-D. Liu, X.-L. Dong, J. Zhang, C.-T. Chen, Z.-Y. Xu, H.-M. Weng, X. Dai, Z. Fang, and X.-J. Zhou, Chin. Phys. Lett. **32**, 067303 (2015).

[20] M. Yan, H. Huang, K. Zhang, E. Wang, W. Yao, K. Deng, G. Wan, H. Zhang, M. Arita, H. Yang, Z. Sun, H. Yao, Y. Wu, S. Fan, W. Duan, and S. Zhou, Nat. Commun. **8**, 257 (2017).

[21] H.-J. Noh, J. Jeong, E.-J. Cho, K. Kim, B. I. Min, and B.-G. Park, Phys. Rev. Lett. **119**, 016401 (2017).

[22] K. Zhang, M. Yan, H. Zhang, H. Huang, M. Arita, Z. Sun, W. Duan, Y. Wu, and S. Zhou, Phys. Rev. B **96**, 125102 (2017).

[23] M. S. Bahramy, O. J. Clark, B. J. Yang, J. Feng, L. Bawden, J. M. Riley, I. Markovic, F. Mazzola, V. Sunko, D. Biswas, S. P. Cooil, M. Jorge, J. W. Wells, M. Leandersson, T. Balasubramanian, J. Fujii, I. Vobornik, J. E. Rault, T. K. Kim, M. Hoesch, K. Okawa, M. Asakawa, T. Sasagawa, T. Eknapakul, W. Meevasana, and P. D. C. King, Nat. Mater. **17**, 21 (2017).

[24] F. Fei, X. Bo, R. Wang, B. Wu, J. Jiang, D. Fu, M. Gao, H. Zheng, Y. Chen, X. Wang, H. Bu, F. Song, X. Wan, B. Wang, and G. Wang, Phys. Rev. B **96**, 041201(R) (2017).

[25] R. C. Xiao, P. L. Gong, Q. S. Wu, W. J. Lu, M. J. Wei, J. Y. Li, H. Y. Lv, X. Luo, P. Tong, X. B. Zhu, and Y. P. Sun, Phys. Rev. B **96**, 075101 (2017).

[26] K. Kudo, H. Ishii, and M. Nohara, Phys. Rev. B **93**, 140505 (2016).

[27] H. Leng, C. Paulsen, Y. K. Huang, and A. de Visser, Phys. Rev. B **96**, 220506 (2017).

[28] S. Das, Amit, A. Sirohi, L. Yadav, S. Gayen, Y. Singh, and G. Sheet, Phys. Rev. B **97**, 014523 (2018).

[29] O. J. Clark, M. J. Neat, K. Okawa, L. Bawden, I. Marković, F. Mazzola, J. Feng, V. Sunko, J. M. Riley, W. Meevasana, J. Fujii, I. Vobornik, T. K. Kim, M. Hoesch, T. Sasagawa, P. Wahl, M. S. Bahramy, and P. D. C. King, Phys. Rev. Lett. **120**, 156401 (2018).

[30] Amit and Y. Singh, Phys. Rev. B **97**, 054515 (2018).

[31] Y. Wang, J. Zhang, W. Zhu, Y. Zou, C. Xi, L. Ma, T. Han, J. Yang, J. Wang, J. Xu, L. Zhang, L. Pi, C. Zhang, and Y. Zhang, Sci. Rep. **6**, 31554 (2016).

[32] A. E. Dunsworth, Low Temp. Phys. **19**, 51 (1975).

[33] See Supplemental Material at http://link.aps.org/supplemental/10.1103/PhysRevB.97.235154 for single-crystal x-ray diffraction precession images of $PdTe_2$, Hall-effect data for $PtTe_2$ and fits to the two-band model, magnetization of $PtTe_2$ as a function of the external field and extraction of its effective masses, Fourier transforms of the oscillatory signal extracted from both compounds as a function of the angle, and a comparison with band structure calculations.

[34] P. Giannozzi, S. Baroni, N. Bonini, M. Calandra, R. Car, C. Cavazzoni, D. Ceresoli, G. L. Chiarotti, M. Cococcioni, I. Dabo *et al.*, J. Phys. Condens. Matter **21**, 395502 (2009).

[35] The Materials Project, https://materialsproject.org.

[36] D. R. Hamann, Phys. Rev. B **88**, 085117 (2013).

[37] A. Kokalj, J. Mol. Graphics Modell. **17**, 176 (1999).

[38] P. Rourke and S. Julian, Comput. Phys. Commun. **183**, 324 (2012).

[39] K. Schwarz, P. Blaha, and G. Madsen, Comput. Phys. Commun. **147**, 71 (2002).

[40] J.-P. Jan and H. L. Skriver, J. Phys. F **7**, 1719 (1977).

[41] D. Rhodes, S. Das, Q. R. Zhang, B. Zeng, N. R. Pradhan, N. Kikugawa, E. Manousakis, and L. Balicas, Phys. Rev. B **92**, 125152 (2015).

[42] K. Wang, D. Graf, and C. Petrovic, Phys. Rev. B **87**, 235101 (2013).

[43] X. Huang, L. Zhao, Y. Long, P. Wang, D. Chen, Z. Yang, H. Liang, M. Xue, H. Weng, Z. Fang, X. Dai, and G. Chen, Phys. Rev. X **5**, 031023 (2015).

[44] Y. Luo, H. Li, Y. M. Dai, H. Miao, Y. G. Shi, H. Ding, A. J. Taylor, D. A. Yarotski, R. P. Prasankumar, and J. D. Thompson, Appl. Phys. Lett. **107**, 182411 (2015).

[45] Q. Zhou, D. Rhodes, Q. R. Zhang, S. Tang, R. Schönemann, and L. Balicas, Phys. Rev. B **94**, 121101 (2016).

[46] W. Gao, N. Hao, F.-W. Zheng, W. Ning, M. Wu, X. Zhu, G. Zheng, J. Zhang, J. Lu, H. Zhang, C. Xi, J. Yang, H. Du, P. Zhang, Y. Zhang, and M. Tian, Phys. Rev. Lett. **118**, 256601 (2017).

[47] D. Shoenberg, *Magnetic Oscillations in Metals* (Cambridge University Press, Cambridge, 1984).

[48] J. Hu, Z. Tang, J. Liu, X. Liu, Y. Zhu, D. Graf, K. Myhro, S. Tran, C. N. Lau, J. Wei, and Z. Mao, Phys. Rev. Lett. **117**, 016602 (2016).

[49] K.-W. Chen, X. Lian, Y. Lai, N. Aryal, Y.-C. Chiu, W. Lan, D. Graf, E. Manousakis, R. E. Baumbach, and L. Balicas, Phys. Rev. Lett. **120**, 206401 (2018).